crystals

MDPI

Article

A Computational Study on Polar $ABiO_3$ (A = Ca, Zn, Mg) Compounds with Large Electric Polarization

Florina Ștefania Rus [1,*] and João Nuno Gonçalves [2,*]

[1] National Institute for Research and Development in Electrochemistry and Condensed Matter, 300569 Timisoara, Romania
[2] CICECO—Aveiro Institute of Materials and Physics Department, Universidade de Aveiro, 10-193 Aveiro, Portugal
* Correspondence: rusflorinastefania@gmail.com (F.Ș.R.); joaonsg@ua.pt (J.N.G.)

Abstract: Bismuth-based oxides with chemical formula $ABiO_3$, where A = Ca, Zn, Mg, have been recently synthesized and suggested to host ferroelectricity. As these materials possess favorable optical properties, the presence of ferroelectricity with large polarization would further enhance the possible applications, for example, in photovoltaics by improving the separation of charge carriers. In this work, first-principles Density Functional Theory (DFT) calculations are performed to study the relative stability of the different polymorphs and to investigate the structural, electronic, and ferroelectric properties. Furthermore, the effect of compressive and tensile in-plane strain on the polarization and electronic properties is also considered. Our study suggests that $CaBiO_3$ should have a large electric polarization (1.8 C/m^2) comparable to the one of $BiFeO_3$. Interestingly, the very high polarization appears with only slightly anomalous values of Born effective charges, which would point out a dominant ionic contribution. Our results call for further studies, both from experimental and theoretical sides, to confirm the large electric polarization $CaBiO_3$ predicted in this work. For $ZnBiO_3$ and $MgBiO_3$, we have demonstrated that, up to large values of strain, the perovskite structure retains favorable ferroelectric and electronic (band gap) properties.

Keywords: ABO3-type perovskite; ferroelectric polarization; strain; non-perovskite

check for updates

Citation: Rus, F.Ș.; Gonçalves, J.N. A Computational Study on Polar $ABiO_3$ (A = Ca, Zn, Mg) Compounds with Large Electric Polarization. *Crystals* **2023**, *13*, 1403. https://doi.org/10.3390/cryst13091403

Academic Editors: Mingqing Liao, Xiaoqiang Liu, Yingchun Ding, Zheng Chang, Jintong Guan, Fei Zhou and Xin Liu

Received: 31 July 2023
Revised: 11 September 2023
Accepted: 18 September 2023
Published: 21 September 2023

Copyright: © 2023 by the authors. Licensee MDPI, Basel, Switzerland. This article is an open access article distributed under the terms and conditions of the Creative Commons Attribution (CC BY) license (https://creativecommons.org/licenses/by/4.0/).

1. Introduction

Ferroelectric materials are characterized by the presence of spontaneous electric polarization, which can be switched by an applied external electric field. A necessary condition for the presence of electric polarization is the non-centrosymmetry of the crystal and a remnant polarization at zero external electric field. There are over 250 materials known to have ferroelectric properties, and a wide range of ferroelectric applications have been considered [1]. The permittivity of ferroelectric materials is very high especially when close to the phase transition temperature, and, therefore, they are used to make capacitors with tunable capacitance. Ferroelectric capacitors comprise a pair of electrodes sandwiching a layer of ferroelectric material. The presence of polarization allows or facilitates carrier separation: electron-hole pairs excited in a ferroelectric are driven apart by the inherent electric field, allowing for the passive collection of energy carriers. Aside from carrier separation, another feature of ferroelectrics that can be used in solar cells is the "anomalous photovoltaic effect," which occurs in inhomogeneous samples, so named because it produces photovoltages 100–1000 times the band gap [2].

Ferroelectric materials have a wide range of useful applications, such as infrared detectors or non-volatile memories due to their bistable polar states [3,4] (for example, using ferroelectric field-effect transistor devices [5,6]). The piezoelectric properties make them useful for actuators, radio frequency filters, sensors, and transducer devices, while ferroelectric capacitors are used due to their good dielectric behavior. They are available in

different forms, such as single crystals, ceramics, thin films, polymers, and composites, according to the necessity of the application. Among the most studied classes of ferroelectrics, the family of perovskite materials certainly has a relevant role.

Perovskite materials such as the calcium titanate ($CaTiO_3$) mineral on which the name perovskite is based, have the prototype undistorted structure with ABX_3 chemical formula and cubic symmetry [7]. A well-studied simple perovskite is barium titanate ($BaTiO_3$), which has a measured spontaneous polarization of 0.21 C/m^2 in the [001] direction in its tetragonal phase [8]. $BaTiO_3$ material is often used as a dielectric in capacitors, and it is a UV-responsive semiconductor photocatalyst due to the relatively large bandgap of 3.4 eV [8]. Ferroelectric materials have shown potential in storage with ferroelectric memories [9] and have notable promise in the field of sustainable energy with ferroelectric photovoltaic devices, which can be improved through the use of nanomaterials [10]. Additionally, ferroelectrics are thought to be promising for overcoming some deficiencies of present photocatalysts, such as charge recombination, surface reaction barriers, and poor light absorption [11]. Wang and colleagues first converted mechanical energy to electricity using piezoelectric ZnO nanowires [12], which sparked the use of non-centrosymmetric materials in photocatalysis. Ferroelectrics and ferroelectric-related compounds have been discovered to have excellent e-h separation and catalytic efficiency in photocatalysis due to internal spontaneous polarization. These materials are also promising semiconductor photocatalyst candidates for reducing water and air pollution, as well as for the energy crisis.

Recently, bismuth-based oxides with the formula $ABiO_3$ (with A alkali or alkaline earth elements) have been studied as photocatalysts for the degradation of undesirable compounds under solar irradiation [13]. They are also expected to have favorable optical absorption properties for photovoltaic applications due to the small band gap and high charge mobilities, which have been recently predicted by a computational study and are associated with the charge disproportionation of bismuth ions [14]. A renewed interest in $ABiO_3$ materials comes also from their superconducting state [15]. Topological nature with Dirac surface states has also been predicted in $ABiO_3$ compounds, in their valence and conduction bands [16,17], due to the covalent interactions in Bi{s,p}-O{p} states between Bi and the octahedral oxygen complex, with bonding states producing the valence topological state and anti-bonding states producing the conduction band state [17].

For $CaBiO_3$, there has been a recent study proposing a highly distorted non-perovskite structure [18]. This structure was found by an evolutionary crystal structure prediction method for zero pressure (Section II. A. 3 of Reference [18]). There are no measurements that allow us to confirm the proposed structure. Only lattice parameters are estimated in nanoflakes [19], which does not allow us to differentiate between the calculated structures and the possible occurrence of a non-polar space group, (as discussed in Section 3). Therefore, we have considered the new distorted $CaBiO_3$ structure for the computational study of its structural, electronic, and ferroelectric properties. Furthermore, we have also investigated the strain effects on $ABiO_3$ materials with A = Ca, Mg, and Zn, which may be relevant for epitaxial thin films.

Our computational study suggests a large polarization for all materials, in particular for $CaBiO_3$, where it is predicted to be 1.8 C/m^2. Variations of in-plane strain suggest that growing thin films in adequate substrates should not affect the band gap, which is favorable for optoelectronic applications while keeping the large values of polarization with moderate variations. However, our computational study does not prove that the actual materials could be synthesized in thin films since we did not consider all possible competing structures or some other effects not included in this discussion, such as the interaction with the substrate. Nevertheless, the calculated properties suggest more detailed experimental investigations of these compounds, particularly the ferroelectric properties.

2. Materials and Methods

We performed density functional theory calculations using QUANTUM ESPRESSO (QE) [20,21]. The pseudopotentials were taken from the SSSP precision v1.1.2 [22] database.

For most calculations, and except noted otherwise, we used the PBEsol [23] exchange-correlation functional. The HSE06 [24,25] hybrid functional has also been used in some cases as a check and for the calculation of more accurate band gaps. We considered a $7 \times 7 \times 3$ k-points grid for Brillouin zone integrations, with the structure in the hexagonal setting. The wave functions were expanded with an energy cutoff of 65 Ry and the density with a cutoff of 520 Ry. The structural optimization stopped when the energy difference between consecutive steps was less than 0.14 meV and the atomic forces were less than 0.26 meV/Å.

The systems considered in this study are $CaBiO_3$, $ZnBiO_3$, and $MgBiO_3$. After the initial structural optimization considering two candidate structures (perovskite and non-perovskite, as detailed in the Section 3), the stable, optimized structures for each composition are used to study the electronic structure and ferroelectric properties. The electronic polarization was calculated using the modern theory with the Berry phase [26,27], and Born effective charge tensors were calculated with Density-Functional Perturbation Theory [28] using the PHonon package (part of QE [20,21]). For calculations with strain, the hexagonal lattice parameters of the structures in their hexagonal setting, $a = b$ were changed between -2% and $+2\%$ (-4% to $+6\%$ in $CaBiO_3$) concerning its optimized value, with the c lattice constant relaxed for each case. All the methods used here can be easily used in other, possibly more complex, compositions, as long as there is a well-defined starting structural model.

3. Results

3.1. $CaBiO_3$

3.1.1. Trigonal Non-Perovskite Structure

We first studied $CaBiO_3$ by considering the trigonal structure which Smolyanyuk et al. found at zero and low pressures using an evolutionary method for crystal structure prediction [18]. This structure has been described as a non-perovskite structure due to the different Bi-Bi and Ca-Ca environments, tetrahedral instead of octahedral [18]. The distorted trigonal structure with the *R3* space group is competing with a perovskite structure previously proposed by He et al. [14]. Smolyanyuk et al. showed that the non-perovskite structure is 12 (PBE) to 17 (HSE) meV/fu lower in energy. Our calculations support the result by Smolyanyuk et al. with a calculated energy difference between non-perovskite and perovskite structures about 77 meV/fu, with the non-perovskite structure more stable. Recently, Xu et al. have calculated the ferroelectric and photocatalytic properties of $CaBiO_3$ [29] for the perovskite structure. Figure 1 shows a planar view of both structures, which are seen to be different in the layering of Ca/Bi atoms along the c axis. While in the perovskite structure, Ca and Bi layers alternate along the c axis, in the non-perovskite structure, two layers of Ca alternate with two layers of Bi.

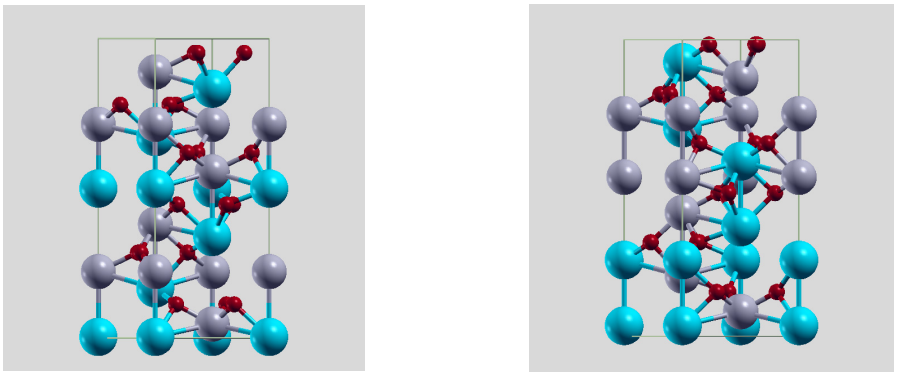

(**a**) (**b**)

Figure 1. Planar view of the perovskite structure from (**a**) He et al. [14] and (**b**) the non-perovskite structure from Smolyanyuk et al. [18] after our structural optimization. Ca atom is shown as blue-spheres, Bi as gray spheres, and O as small red spheres.

We first performed a structural optimization with the PBEsol exchange-correlation approximation, starting from the predicted non-perovskite structure of Reference [18]. For further checks, we performed the structural optimization with both QE and VASP, obtaining similar values for the lattice parameters in both codes, as shown in Table 1. The small difference between our values and Reference [18] is expected since they used PBE while we used the PBEsol approximation. Khosya et al. [19] have synthesized $CaBiO_3$ nanoflakes, with lattice parameters estimated at a = 5.81 and c = 15.50 Å. The lattice parameters are in reasonable agreement with our estimate: while *a* is very close, *c* is underestimated (−4.5%); however, they have assigned the structure to the $R\bar{3}c$ space group, which is non-polar and it does not fit from the *R*3 group space. They have measured a small polarization of 0.02 μC cm^{-2}, which is nonconsistent with the non-polar space group assignment. This calls for more structural and ferroelectric characterizations on this compound.

Table 1. Optimized lattice parameters of $CaBiO_3$, with the trigonal non-perovskite structure from Smolyanyuk et al. [18] (first row) or after variable cell relaxation with PBEsol approximation (QE and VASP codes).

Method/Lattice Parameters	*a* (Å)	*c* (Å)
PBE, previous work [18]	5.92	15.17
PBEsol, QE	5.85	14.85
PBEsol, VASP (PAW method)	5.86	14.87

Figure 2 presents the calculated density of states (DOS) using the PBEsol relaxed structure. The shape of the DOS is similar to the HSE06 functional but the band gap is 1.8 eV with PBEsol and 3.2 eV with HSE. As expected, the PBEsol underestimates the band gap with respect to the HSE06. The perovskite structure has a smaller band gap of 1.58 eV as calculated with HSE [14] and mBJ [29] functionals.

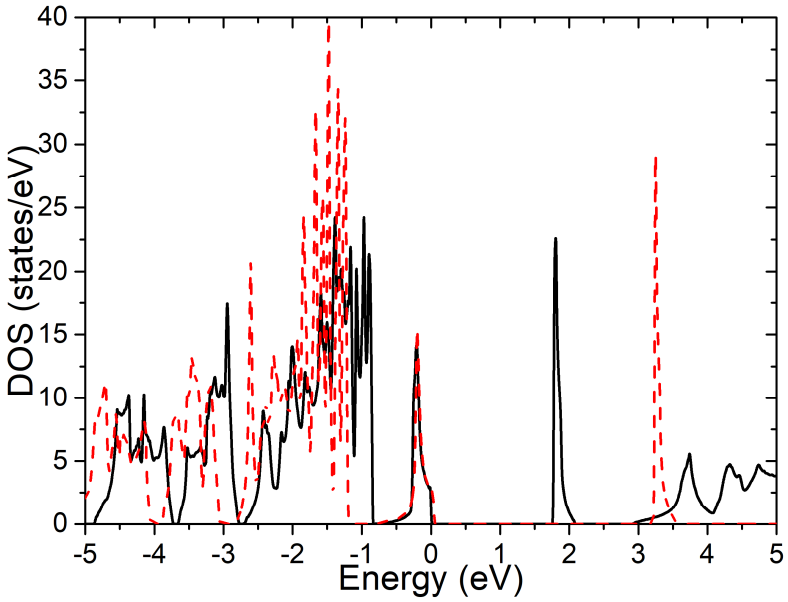

Figure 2. The electronic total density of states calculated with PBEsol (black line) and HSE (red dashed line).

Figure 3 shows the spontaneous polarization of the same structure relative to a reference higher symmetry structure (space group R−3) obtained from the PSEUDO tool of the Bilbao Crystallographic Server [30,31].

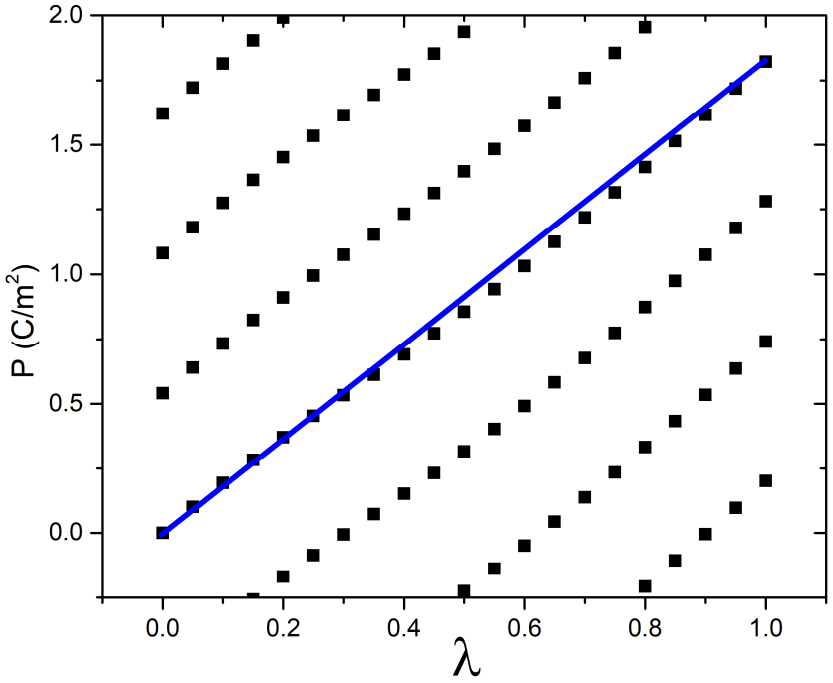

Figure 3. Polarization lattice as a function of a distortion parameter between the centrosymmetric reference structure R-3 and the calculated trigonal structure for non-perovskite $CaBiO_3$. The blue line is the choice of points to calculate the polarization variation, which results in ΔP = 1.82 C/m^2.

Due to the multi-valuedness of the bulk polarization [26,27], with the polarization quantum equal to 0.54 C/m^2, several points are considered in the polarization path, from the centrosymmetric space group *R*-3 ($\lambda = 0$) to the non-perovskite structure *R*3 to remove the ambiguity. The calculated polarization difference is shown by the blue line and amounts to 1.82 C/m^2 (or 182 μC/cm^2) along the [001] direction in the hexagonal setting, which is a very high value when compared with most ferroelectric compounds. For example, $BiFeO_3$ is known to have a very high polarization ~1.0 C/m^2, which is still much smaller than the value calculated here. We checked the polarization with the VASP code and PAW method, with the optimized VASP lattice parameters shown in Table 1 (very similar to the QE parameters), and obtained the same final total polarization difference. Materials with high polarization would benefit applications such as ferroelectric random-access memories (FeRAM) and capacitors [32].

3.1.2. Born Effective Charges

To investigate the origin of the polarization, we calculated the Born effective charge tensors (BEC), defined as $Z^*_{k,\alpha\beta} = (\Omega/e)\partial P_\alpha / \partial u_{k,\beta}$ where P_α is the polarization in direction α, $u_{k,\beta}$ is the displacement of atom k in direction β, Ω is the primitive cell volume, and e is the elementary charge. Table 2 presents the eigenvalues of the BEC tensors in $CaBiO_3$ (computed with numpy [33], for example). Due to the low symmetry in the structure, some eigenvalues are complex but with small imaginary components. We focus on the real values. We see that the charges are close to +4 for Bi, +2.7 for Ca, and −3 for O. They can be compared with the nominal ionic charges of +4 for Bi, +2 for Ca, and −2 for O. The charges are somewhat anomalous, with slightly higher values than formal ionic charges for Ca and O ions, but they are not highly anomalous as in other perovskite oxides. This indicates that the polarization is due, in large part, to the geometric distortion, with a less important component due to hybridization changes.

Table 2. BEC eigenvalues ($\lambda_{1,2,3}$), in *e* units, for non-perovskite $CaBiO_3$ with PBEsol approximation.

BEC Eigenvalues	λ_3	λ_2	λ_1
Z*(Bi1)	4.22 + 0.33i	4.22 − 0.33i	4.50
Z*(Bi2)	3.94 + 0.37i	3.94 − 0.37i	5.29
Z*(Ca1)	2.88 + 0.46i	2.88 − 0.46i	2.35
Z*(Ca2)	2.65 + 0.23i	2.65 − 0.23i	2.15
Z*(O1)	−3.38	−1.52	−2.18
Z*(O2)	−2.89	−2.39	−1.54

3.1.3. Strain

We investigated the application of in-plane strain, which could model the growth of epitaxial thin films in different substrates. The out-of-plane lattice parameter and the atomic positions are fully relaxed for each strain state with the PBEsol approximation.

There are small changes in both the total DOS and band gap with strain, as shown in Figures 4 and 5. The band gap is largest at ~1.8 eV for the unstrained structure and decreases a bit to 1.6–1.7 eV for strained structures. The center of valence states is slightly pushed up to the Fermi level with increasing tensile strain, as can be seen by the decreasing gap between the peak just before the Fermi level and the wide band before that peak. The same happens in other oxides [34].

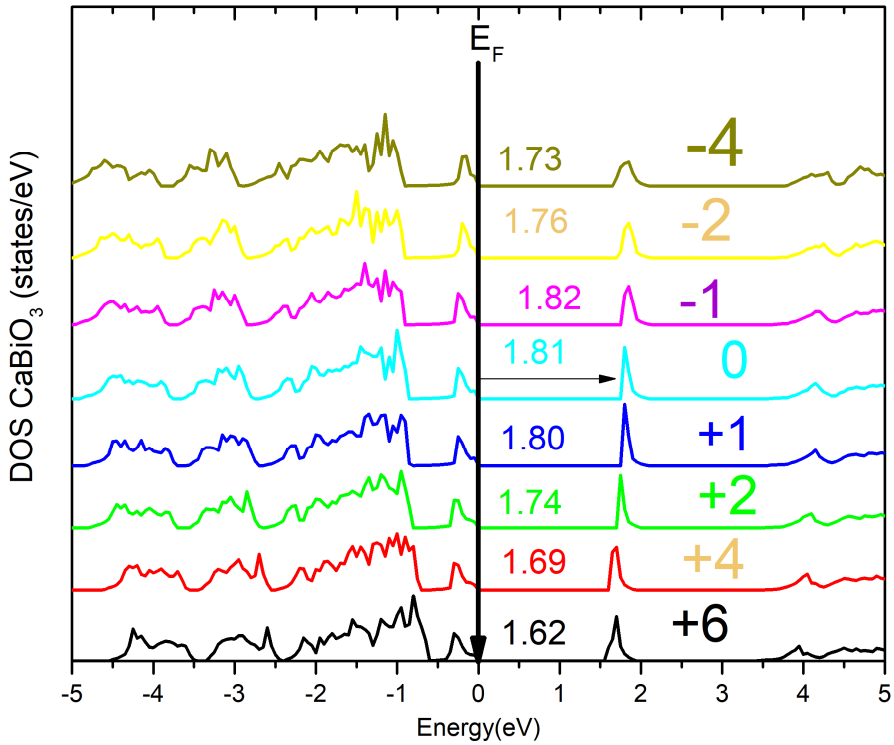

Figure 4. Total electronic density of states for non-perovskite $CaBiO_3$. The zero energy is the top of the valence band, the band gap (eV) is shown by the numbers, and strain states are shown in % relative to the unstrained $a = b$ lattice parameter.

On the other hand, the polarization has more significant changes with strain. The 1.8 C/m^2 value of the unstrained structure increases to 2 C/m^2 with compressive in-plane strain and decreases to 1.6 C/m^2 with tensile strain of a few percent, as shown in Figure 6.

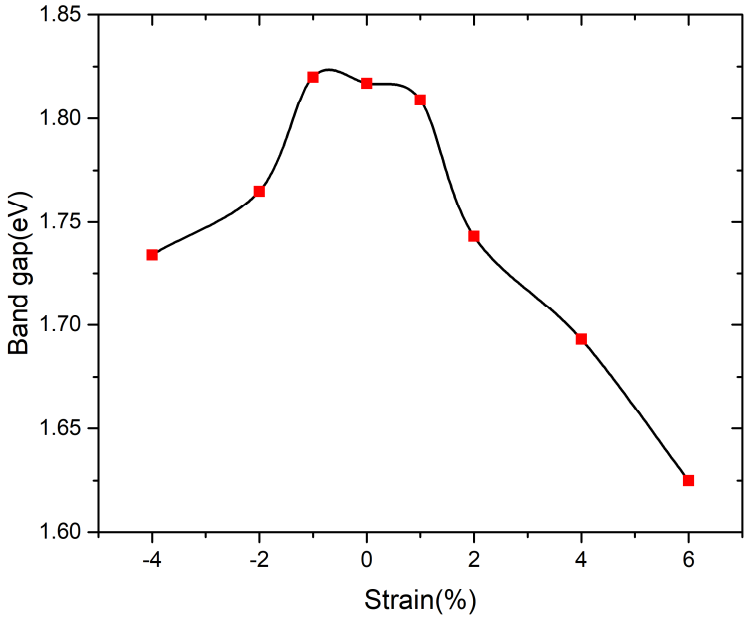

Figure 5. Band gap (eV) as a function of the in-plane strain for non-perovskite $CaBiO_3$.

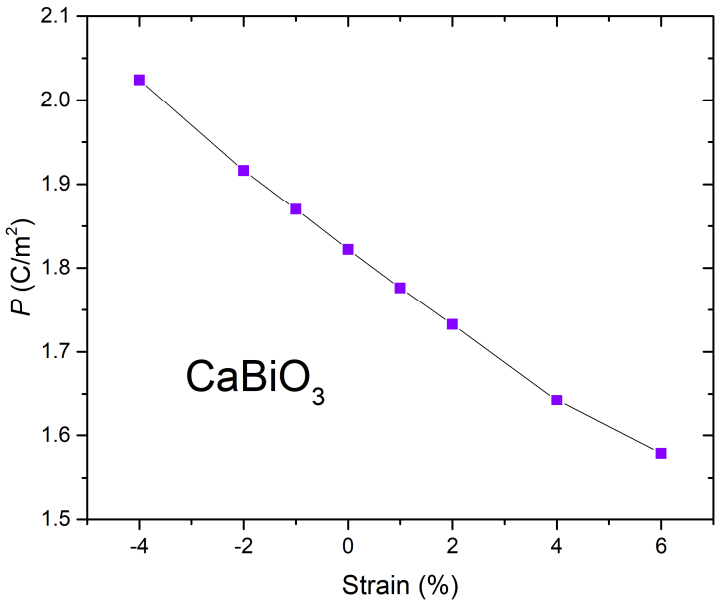

Figure 6. Spontaneous polarization as a function of the in-plane strain for non-perovskite $CaBiO_3$.

3.2. $ZnBiO_3$ and $MgBiO_3$

For $MgBiO_3$ and $ZnBiO_3$, we first tested the trigonal distorted variant found for $CaBiO_3$ also in these compositions by starting from the $CaBiO_3$ structure, replacing the A site, and optimizing within PBEsol. In these cases, the perovskite-derived structure (as calculated by He et al. [14]) was found to have lower energy, by 87 meV/fu for $MgBiO_3$ and 147 meV/fu for $ZnBiO_3$. Then, we continued with the perovskite *R*3 structure for a more detailed study. The optimized bulk lattice parameters (a = 5.47, c = 14.58 Å for $MgBiO_3$, a = 5.50, c = 14.62 Å for $ZnBiO_3$) are similar to the ones obtained by He et al. (a = 5.48, c = 14.60 Å for $MgBiO_3$, a = 5.51, c = 14.65 Å for $ZnBiO_3$) [14].

Figure 7 shows the band gap obtained with PBEsol for in-plane strains. The zero strain values of 0.89 eV for $ZnBiO_3$ and 0.97 eV are close to the PBEsol values of He et al. [14] (0.86 eV and 0.94 eV, respectively). The results show that the band gap variation is small, within 0.06 eV.

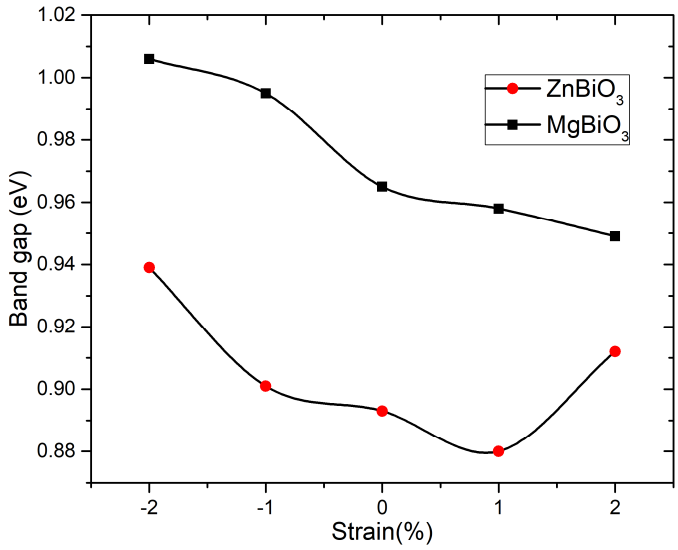

Figure 7. Bandgap (eV) as a function of the in-plane strain for perovskites $ZnBiO_3$ and $MgBiO_3$.

The variation of spontaneous polarization is shown in Figure 8. The results are in qualitative agreement with Reference [14] for zero strain, confirming their estimation—where the BEC tensors and the distortion are used to estimate the polarization.

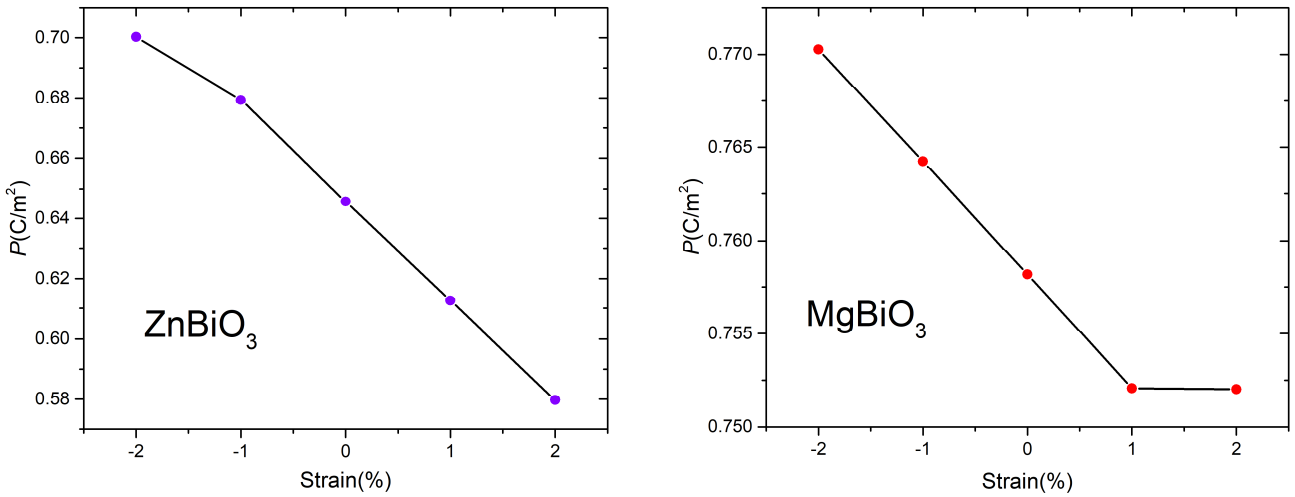

(**a**) (**b**)

Figure 8. Polarization as a function of in-plane strain (%) relative to the optimized PBEsol structure (0%) for (**a**) $ZnBiO_3$ and (**b**) $MgBiO_3$.

While He et al. [14] estimated the polarization based on BECs, they did not discuss them. To better understand the origin of the polarization, in Tables 3 and 4, we report the obtained BECs for $ZnBiO_3$ and $MgBiO_3$, respectively. The BEC principal components are slightly more anomalous here than in the $CaBiO_3$ distorted structure, with O components -3.2 to -3.8 |e|. There is a larger difference between the inequivalent Bi atoms (1 to 1.3 |e| difference) when compared to 0.3 |e| in $CaBiO_3$. The polarization change as a function of strain is shown in Figure 7. It has very small changes in $MgBiO_3$ (0.75 to 0.77 C/m^2) and greater changes in $ZnBiO_3$ (0.58 to 0.70 C/m^2). $CaBiO_3$ with the non-perovskite structure still has the higher change of polarization in this interval of strain (1.55 to 2.05 C/m^2 between -2% and +2% strain). Compared with well-known ferroelectric oxides [35], the large change of $CaBiO_3$ is closer to the $BaTiO_3$ and $PbTiO_3$ changes (though not so high in relative terms), while the smaller changes of $ZnBiO_3$ and $MgBiO_3$ are closer

to the $LiNbO_3$ and $BiFeO_3$ (*R*3*c*) cases. To summarize, concerning previous works [14,18], we present additional detailed calculations of the predicted structures for its electronic structure and band gap, BECs, and variation of polarization and band gaps with strain, which is important to predict the possible tuning of functionalities with the growth of thin films on appropriate substrates.

Table 3. BEC eigenvalues ($\lambda_{1,2,3}$), in *e* units, for perovskite $ZnBiO_3$ with PBEsol approximation.

BEC Eigenvalues	λ_3	λ_2	λ_1
Z*Bi1	4.22	4.92 − 0.62i	4.92 + 0.62i
Z*Bi2	5.53	5.02 − 1.02i	5.02 + 1.02i
Z*Zn1	2.36	2.51 − 0.24i	2.51 + 0.24i
Z*Zn2	2.14	2.48 − 0.25i	2.48 + 0.25i
Z*O1	−3.84	−2.15	−1.66
Z*O2	−3.36	−1.53	−2.17

Table 4. BEC eigenvalues ($\lambda_{1,2,3}$), in *e* units, for perovskite $MgBiO_3$ with PBEsol approximation.

BEC Eigenvalues	λ_3	λ_2	λ_1
Z*(Bi1)	4.012	4.90 − 0.81i	4.90 + 0.81i
Z*(Bi2)	5.49	4.83 − 1.26i	4.83 + 1.26i
Z*(Mg1)	2.06	2.15 − 0.44i	2.15 + 0.44i
Z*(Mg2)	1.91	2.17 − 0.38i	2.17 + 0.38i
Z*(O1)	−3.77	−1.59	−1.75
Z*(O2)	−3.22	−1.50	−2.01

The main new results of this work are in two points: (i) for CaBiO3, the detailed calculation of the non-perovskite structure, confirming its stability and showing it has much higher polarization than the perovskite structure, which should encourage more detailed experimental studies on this compound in the future to confirm or disprove this structure and its properties; (ii) for ZnBiO3 and MgBiO3, we have shown that, up to large values of strain, the perovskite structure retains favorable ferroelectric and electronic properties, which should encourage the study of these materials also in epitaxial thin film form.

4. Discussion

First-principles calculations confirm the non-perovskite structure for $CaBiO_3$ and the perovskite-derived structure for $MgBiO_3$ and $ZnBiO_3$. The polarization is very high in $CaBiO_3$, and the variations with in-plane strain are also higher than for Mg/Zn compounds, nevertheless keeping a high polarization for reasonable strain variations in all materials. The electronic structure and band gap, on the other hand, show only small changes up to strains of about 4%. The giant polarization predicted for $CaBiO_3$ makes it a particularly interesting material for future studies, which requires experimental confirmation. The Born effective charges indicate the origin of the polarization to be due to electronic changes as well as geometric displacements in all materials.

Author Contributions: F.Ș.R. suggested the topic and wrote the HPC project. J.N.G. supervised the project. All authors have read and agreed to the published version of the manuscript.

Funding: This work was performed under the project HPC-EUROPA3 (INFRAIA-2016-1-730897) with the support of the EC Research Innovation Action under the H2020 Programme; the authors gratefully acknowledge the support of Alessandro Stroppa and the hospitality from CNR -SPIN c/o Department of Physical and Chemical Sciences, University of L'Aquila, Via Vetoio, I-67100, Coppito, L'Aquila, Italy. We are grateful for the computer resources and technical support provided by CINECA. J.N.G. worked within the scope of the project CICECO-Aveiro Institute of Materials, UIDB/50011/2020 and UIDP/50011/2020, financed by national funds through the Portuguese Foundation for Science and Technology/MCTES.

Data Availability Statement: The data presented in this study are available on request from the corresponding authors.

Conflicts of Interest: The authors declare no conflict of interest.

References

1. Said, S.M.; Sabri, M.F.M.; Salleh, F. Ferroelectrics and Their Applications. In *Reference Module in Materials Science and Materials Engineering*; Elsevier: Amsterdam, The Netherlands, 2017; ISBN 978-0-12-803581-8.
2. Butler, K.T.; Frost, J.M.; Walsh, A. Ferroelectric Materials for Solar Energy Conversion: Photoferroics Revisited. *Energy Environ. Sci.* **2015**, *8*, 838–848. [CrossRef]
3. Lines, M.E.; Glass, A.M.; Lines, M.E.; Glass, A.M. *Principles and Applications of Ferroelectrics and Related Materials*; Oxford Classic Texts in the Physical Sciences; Oxford University Press: Oxford, UK; New York, NY, USA, 2001; ISBN 978-0-19-850778-9.
4. Martin, L.W.; Rappe, A.M. Thin-Film Ferroelectric Materials and Their Applications. *Nat. Rev. Mater.* **2016**, *2*, 16087. [CrossRef]
5. Sadabad, Y.A.; Khodadadian, A.; Istadeh, K.H.; Hedayati, M.; Kalantarinejad, R.; Heitzinger, C. Frequency Dependence of Dielectrophoretic Fabrication of Single-Walled Carbon Nanotube Field-Effect Transistors. *J. Comput. Electron.* **2020**, *19*, 1516–1526. [CrossRef]
6. Khodadadian, A.; Parvizi, M.; Teshnehlab, M.; Heitzinger, C. Rational Design of Field-Effect Sensors Using Partial Differential Equations, Bayesian Inversion, and Artificial Neural Networks. *Sensors* **2022**, *22*, 4785. [CrossRef] [PubMed]
7. Lemanov, V.V.; Sotnikov, A.V.; Smirnova, E.P.; Weihnacht, M.; Kunze, R. Perovskite CaTiO3 as an Incipient Ferroelectric. *Solid State Commun.* **1999**, *110*, 611–614. [CrossRef]
8. Razak, N.A.A.; Zabidi, N.A.; Rosli, A.N. A First Principle Study of Band Structure of Tetragonal Barium Titanate. *AIP Conf. Proc.* **2017**, *1875*, 020017. [CrossRef]
9. Mikolajick, T.; Schroeder, U.; Slesazeck, S. The Past, the Present, and the Future of Ferroelectric Memories. *IEEE Trans. Electron. Devices* **2020**, *67*, 1434–1443. [CrossRef]
10. Han, X.; Ji, Y.; Yang, Y. Ferroelectric Photovoltaic Materials and Devices. *Adv. Funct. Mater.* **2022**, *32*, 2109625. [CrossRef]
11. Liu, L.; Huang, H. Ferroelectrics in Photocatalysis. *Chem. Eur. J.* **2022**, *28*, e202103975. [CrossRef]
12. Wang, Z.L.; Song, J. Piezoelectric Nanogenerators Based on Zinc Oxide Nanowire Arrays. *Science* **2006**, *312*, 242–246. [CrossRef]
13. Karuppannan, R.; Sakar, M. Calcium Bismuthate ($CaBiO_3$): A Potential Sunlight-Driven Perovskite Photocatalyst for the Degradation of Emerging Pharmaceutical Contaminants. *ChemPhotoChem* **2020**, *4*, 373–380.
14. He, J.; Franchini, C.; Rondinelli, J.M. Ferroelectric Oxides with Strong Visible-Light Absorption from Charge Ordering. *Chem. Mater.* **2017**, *29*, 2445–2451. [CrossRef]
15. Kuentzler, R.; Hornick, C.; Dossman, Y.; Wegner, S.; El Farsi, R.; Drillon, M. Superconductivity of Pb, K and Rb-Doped $BaBiO_3$. *Phys. C Supercond.* **1991**, *184*, 316–320. [CrossRef]
16. Li, G.; Yan, B.; Thomale, R.; Hanke, W. Topological Nature and the Multiple Dirac Cones Hidden in Bismuth High-Tc Superconductors. *Sci. Rep.* **2015**, *5*, 10435. [CrossRef]
17. Khamari, B.; Kashikar, R.; Nanda, B.R.K. Topologically Invariant Double Dirac States in Bismuth-Based Perovskites: Consequence of Ambivalent Charge States and Covalent Bonding. *Phys. Rev. B* **2018**, *97*, 045149. [CrossRef]
18. Smolyanyuk, A.; Franchini, C.; Boeri, L. Ab-Initio Study of $ABiO_3$ (A = Ba, Sr, Ca) under High Pressure. *Phys. Rev. B* **2018**, *98*, 115158. [CrossRef]
19. Khosya, M.; Faraz, M.; Khare, N. Enhanced Photocatalytic Reduction of Hexavalent Chromium by Using Piezo-Photo Active Calcium Bismuth Oxide Ferroelectric Nanoflakes. *New J. Chem.* **2022**, *46*, 12244–12251. [CrossRef]
20. Giannozzi, P.; Baroni, S.; Bonini, N.; Calandra, M.; Car, R.; Cavazzoni, C.; Ceresoli, D.; Chiarotti, G.L.; Cococcioni, M.; Dabo, I.; et al. QUANTUM ESPRESSO: A Modular and Open-Source Software Project for Quantum Simulations of Materials. *J. Phys. Condens. Matter* **2009**, *21*, 395502. [CrossRef]
21. Giannozzi, P.; Andreussi, O.; Brumme, T.; Bunau, O.; Buongiorno Nardelli, M.; Calandra, M.; Car, R.; Cavazzoni, C.; Ceresoli, D.; Cococcioni, M.; et al. Advanced Capabilities for Materials Modelling with Quantum ESPRESSO. *J. Phys. Condens. Matter* **2017**, *29*, 465901. [CrossRef]
22. Prandini, G.; Marrazzo, A.; Castelli, I.E.; Mounet, N.; Marzari, N. Precision and Efficiency in Solid-State Pseudopotential Calculations. *Npj Comput. Mater.* **2018**, *4*, 72. [CrossRef]
23. Perdew, J.P.; Ruzsinszky, A.; Csonka, G.I.; Vydrov, O.A.; Scuseria, G.E.; Constantin, L.A.; Zhou, X.; Burke, K. Restoring the Density-Gradient Expansion for Exchange in Solids and Surfaces. *Phys. Rev. Lett.* **2008**, *100*, 136406. [CrossRef] [PubMed]

24. Heyd, J.; Scuseria, G.E.; Ernzerhof, M. Hybrid Functionals Based on a Screened Coulomb Potential. *J. Chem. Phys.* **2003**, *118*, 8207–8215. [CrossRef]
25. Krukau, A.V.; Vydrov, O.A.; Izmaylov, A.F.; Scuseria, G.E. Influence of the Exchange Screening Parameter on the Performance of Screened Hybrid Functionals. *J. Chem. Phys.* **2006**, *125*, 224106. [CrossRef] [PubMed]
26. King-Smith, R.D.; Vanderbilt, D. Theory of Polarization of Crystalline Solids. *Phys. Rev. B* **1993**, *47*, 1651–1654. [CrossRef]
27. Resta, R. Macroscopic Polarization in Crystalline Dielectrics: The Geometric Phase Approach. *Rev. Mod. Phys.* **1994**, *66*, 899–915. [CrossRef]
28. Baroni, S.; de Gironcoli, S.; Dal Corso, A.; Giannozzi, P. Phonons and Related Crystal Properties from Density-Functional Perturbation Theory. *Rev. Mod. Phys.* **2001**, *73*, 515–562. [CrossRef]
29. Xu, X.-F.; Chen, L.-F.; Xu, H.-K.; Lai, G.-X.; Hu, S.-M.; Ji, H.; Tang, J.-J.; Chen, X.-Y.; Zhu, W.-L. Theoretical Study on the Stability, Ferroelectricity and Photocatalytic Properties of $CaBiO_3$. *RSC Adv.* **2022**, *12*, 30764–30770. [CrossRef]
30. Aroyo, M.I.; Kirov, A.; Capillas, C.; Perez-Mato, J.M.; Wondratschek, H. Bilbao Crystallographic Server. II. Representations of Crystallographic Point Groups and Space Groups. *Acta Crystallogr. A* **2006**, *62*, 115–128. [CrossRef]
31. Capillas, C.; Tasci, E.S.; de la Flor, G.; Orobengoa, D.; Perez-Mato, J.M.; Aroyo, M.I. A New Computer Tool at the Bilbao Crystallographic Server to Detect and Characterize Pseudosymmetry. *Z. Für Krist. Cryst. Mater.* **2011**, *226*, 186–196. [CrossRef]
32. Mikolajick, T.; Slesazeck, S.; Mulaosmanovic, H.; Park, M.H.; Fichtner, S.; Lomenzo, P.D.; Hoffmann, M.; Schroeder, U. Next Generation Ferroelectric Materials for Semiconductor Process Integration and Their Applications. *J. Appl. Phys.* **2021**, *129*, 100901. [CrossRef]
33. Harris, C.R.; Millman, K.J.; van der Walt, S.J.; Gommers, R.; Virtanen, P.; Cournapeau, D.; Wieser, E.; Taylor, J.; Berg, S.; Smith, N.J.; et al. Array Programming with NumPy. *Nature* **2020**, *585*, 357–362. [CrossRef] [PubMed]
34. Hwang, J.; Feng, Z.; Charles, N.; Wang, X.R.; Lee, D.; Stoerzinger, K.A.; Muy, S.; Rao, R.R.; Lee, D.; Jacobs, R.; et al. Tuning Perovskite Oxides by Strain: Electronic Structure, Properties, and Functions in (Electro)Catalysis and Ferroelectricity. *Mater. Today* **2019**, *31*, 100–118. [CrossRef]
35. Ederer, C.; Spaldin, N.A. Effect of Epitaxial Strain on the Spontaneous Polarization of Thin Film Ferroelectrics. *Phys. Rev. Lett.* **2005**, *95*, 257601. [CrossRef] [PubMed]

Disclaimer/Publisher's Note: The statements, opinions and data contained in all publications are solely those of the individual author(s) and contributor(s) and not of MDPI and/or the editor(s). MDPI and/or the editor(s) disclaim responsibility for any injury to people or property resulting from any ideas, methods, instructions or products referred to in the content.